Classification of Transfer Modes in Gas Metal Arc Welding Using Acoustic Signal Analysis

Mitchell Cullen (Mitchell.C.Cullen@student.uts.edu.au)
University of Technology Sydney https://orcid.org/0000-0002-8104-8772

Sipei Zhao
Centre for Audio, Acoustics, and Vibration, Faculty of Engineering and IT, University of Technology Sydney, 15 Broadway, Ultimo, NSW 2007, Australia

Jinchen Ji
Centre for Audio, Acoustics, and Vibration, Faculty of Engineering and IT, University of Technology Sydney, 15 Broadway, Ultimo, NSW 2007, Australia

Xiaojun Qiu
Centre for Audio, Acoustics, and Vibration, Faculty of Engineering and IT, University of Technology Sydney, 15 Broadway, Ultimo, NSW 2007, Australia

Research Article

Keywords: GMAW, Acoustic Sensing, Transfer Mode, Automated Welding

Posted Date: February 15th, 2021

DOI: https://doi.org/10.21203/rs.3.rs-234787/v1

Classification of Transfer Modes in Gas Metal Arc Welding using Acoustic Signal Analysis

Manuscript submitted for the consideration of publication in the International Journal of Advanced Manufacturing Technology

Mitchell Cullen, Sipei Zhao*, Jinchen Ji, Xiaojun Qiu

Centre for Audio, Acoustics, and Vibration, Faculty of Engineering and IT, University of Technology Sydney, 15 Broadway, Ultimo, NSW 2007, Australia

Email: mitchell.c.cullen@student.uts.edu.au, Sipei.Zhao@.uts.edu.au, jin.ji@uts.edu.au

Total number of pages including this cover page: 30

Total number of figures: 8

Total number of tables: 6

* Corresponding author: Sipei.Zhao@.uts.edu.au

Classification of Transfer Modes in Gas Metal Arc Welding using Acoustic Signal Analysis

Mitchell Cullen, Sipei Zhao*, Jinchen Ji, Xiaojun Qiu

Centre for Audio, Acoustics, and Vibration, Faculty of Engineering and IT, University of Technology Sydney, 15 Broadway, Ultimo, NSW 2007, Australia

* Corresponding author: Sipei.Zhao@.uts.edu.au

Abstract

Gas Metal Arc Welding (GMAW) is a welding process in which an electric arc is formed between a wire electrode and a metal work piece alongside a shielding gas to protect the arc from contaminants. There are several ways in which the molten electrode droplet can be transferred to the weld pool known as metal transfer modes. Identifying the metal transfer mode automatically is essential to monitor and control the welding process, especially in automated processes employed in modern Industry 4.0 manufacturing lines. However, limited research on this topic has been found in literature. This paper explores automatic classification of metal transfer modes in GMAW based on machine learning techniques with various signals from the welding process, including acoustics, current, voltage, and gas flow rate signals. Time and frequency domain features are first extracted from these signals and are used in a support vector machine classifier to detect the metal transfer modes. A feature selection algorithm is proposed to improve the prediction rate from 80% to 99% when all the four signals are utilized. When only the non-intrusive acoustic signal is used, the prediction rates with and without the proposed feature selection algorithm are approximately 96% and 81%, respectively. The high prediction rate demonstrates the feasibility and promising accuracy of the acoustic signal based classification method for future smart welding technology with real-time adaptive feedback control of the welding process.

Keywords:

GMAW, Acoustic Sensing, Transfer Mode, Automated Welding

1. Introduction

Gas Metal Arc Welding (GMAW) is the welding process in which an electric arc is formed between a wire electrode and a metal work piece that generates enough heat to melt the metals together. The process also involves using a gas shielding to protect the weld from contaminants in the air. In GMAW, the molten droplets are transferred from the electrode tip into the molten weld pool along the electric welding arc in a number of different modes, depending on factors such as the droplet size, growth time and detachment frequency [1]. Metal transfer modes are a critical factor in the final quality of the weld, by effecting the weld bead penetration, heat transfer and material deposition rate of the welding process. The transfer modes are influenced by a number of different welding parameters including the welding current, voltage, stick out distance, electrode material, shielding gas composition, wire feed speed, welding speed and material composition [2]. A timely identification of transfer modes can provide vital information to analyze weld quality and to develop smart welding technology, enabling development of an adaptive feedback system to realize the full automation of the welding process.

Various transfer modes have been noted in the GMAW process to occur under different welding parameters. The first major contribution to classifying GMAW transfer modes was the International Institute of Welding (IIW) classification model [3], which shows the relationship between the transfer modes as the welding current increases, changing from the short circuit transfer modes to globular and spray transfers. This model also shows the presence of the theoretical transition current between the globular and spray transfer modes. The relationship between this transition current and the droplet size was investigated by Kim and Eager [4], where the transition between globular and spray transfer mode was found to be a more gradual process than originally outlined in the IIW classification. This model was later improved upon by Iordachescu and Quintino [5], who introduced the presence of a second transition current between globular and short circuit transfer modes as well as introducing additional sub classifications of the major transfer mode categories. Scotti et al. [1] developed a new classification categorizing a new type of transfer mode, known as an interchangeable mode, which

switches between previously established transfer modes. They further classified these interchangeable transfer modes into smaller subgroups [6].

On the other hand, in the welding industry it has been well documented that expert welders are able to distinguish the metal transfer modes by listening to the sound generated by the welding arc and use this to control the welding process accordingly [7]. Experiments by Tam and Huissoon [8] showed further evidence to this by performing psychoacoustic experiments on welders to determine how the welding sound affects their ability to control the welding arc. It was found that when the acoustic signal was delayed by 400 ms, the welders no longer had the ability to control the welding process effectively. These results inspired the current work to investigate the feasibility of metal transfer mode identification based on acoustic signals in GMAW processes.

To understand the sound generation mechanism in GMAW processes and explore its applications in welding process monitoring and quality control, various theoretical and experimental studies have been conducted in the past decades [9]. One of the earliest studies in this area was carried out by Jolly [10], who used the acoustic signal to locate defects in Gas Tungsten Arc Welding (GTAW). Several decades later, Carlson et al. [11] investigated the GMAW sound signal using piezoelectric sensors, in addition to the current and voltage signals, as a means to investigate the relationship between the three signals and the welding droplet detachments. Saini and Floyd [12] also utilized the sound signals to investigate GMAW parameters and transfer modes, where both time and frequency domain features of the sound signal were found to be potential indicators of GMAW transfer modes. Research undertaken by Grad et al. [13] employed the sound signal for online GMAW process monitoring and found that the major source of acoustic emission is generated by the arc re-ignition in short circuit transfer mode. They also discovered that shielding gas composition also had a large impact on acoustic signal parameters. Cayo and Alfaro [14] also used time and frequency domain features of the sound signal to detect possible defects in GMAW welds and found that time domain features were particularly useful in defect detection. Zhang et al. [15] used the acoustic emissions alongside air coupled ultrasonics to classify the degree of burn through in GTAW in real time. Similarly Chen et al. [16] also used the sound signal generated in pulsed GTAW to detect the penetration level of the weld

bead using a dynamic long short-term memory (DLSTM) network model. Recently, Zhao et al. [17] investigated the peaks of the sound signal in GMAW and found that the peak sound pressure, impulse interval and event duration are good indicators of GMAW transfer modes.

In addition to investigating the relationship between the features of the sound signal and the GMAW process, machine learning algorithms have also been used to predict welding features in GMAW. Tam [18] used artificial neural networks to predict the welding parameters from the acoustic signal. Wang and Huissoon [19] used artificial neural networks with a naïve Bayesian classifier to classify the transfer modes using the acoustic signal. Similarly, Rudas et al. [20] developed both a grey and black box model using neural networks to predict the transfer modes and found that it was difficult to classify the transfer modes between the transition from globular to spray mode due to the instability of the welding arc. Lv et al. [21] developed an online weld penetration detection system using neural networks based around the acoustic signal. Despite the previous research which has shown the significance of the acoustic signal in defect detection and process monitoring in GMAW, there is still limited research in automatic and effective detection system that can differentiate between the numerous transfer modes [22].

As mentioned above, the metal transfer mode is a key factor that determines the weld quality, thus an automatic transfer mode classification system is desired for quality control in GMAW processes. Furthermore, identifying metal transfer modes automatically with acoustic sensing and analysis can be used to provide real-time adaptive feedback control for automated robotic welding, which will lay a solid foundation for further development of a smart welding facility, such as a portable device either individually or to be integrated into other real-time monitoring systems in manufacturing industry, in particular in hazardous environments.

This paper investigates the application of acoustic sensing on automatic real-time metal transfer mode identification. A multi-sensor measurement system is developed to simultaneously measure the welding current, arc voltage, gas flow rate and acoustic signals, from which various time and frequency domain features are extracted and selected to train a Support Vector Machine (SVM) classifier for metal transfer mode identification. The SVM classifiers for the 4 different signals are

compared to evaluate their performance. A feature selection algorithm is developed to reduce the feature dimensionality and improve accuracy. The results demonstrate the feasibility of automatic metal transfer mode identification based on various signals, among which the acoustic sensing based approach has a distinct advantage over the others due to its non-intrusiveness and ease of installation, making it a promising plug-and-play solution for GMAW processes.

2. Experimental apparatus and procedure

2.1 Experimental setup

Fig. 1 shows the experimental setup that was used to perform the GMAW while recording the acoustic, current, voltage and gas flow rate signals. In the experiments, a Lincoln Electric PowerWave C300 MIG welder was used with the torch mounted above a servo driven workbench. To perform all of the welds, the welding torch was fixed above the work piece, with the work piece being driven forward at a fixed speed by the servo motor. In all of the performed tests a 0.9 mm electrode wire was used in combination with a pure argon gas mixture for the welding gas. A steel plate was used as a work piece with each weld being performed for approximately 40 seconds.

To record the acoustic signal, a GRAS 40PH free-field microphone was mounted 480 mm above the welding torch. The current signal was measured using an LEM HTA 300-S current sensor mounted around the welding torch cable while the voltage signal was obtained directly from the positive welding torch and the negative workbench. The gas flow rate signal was recorded using a gas flow sensor mounted before the welding torch.

All signals were captured using a National Instruments cDAQ 9185 chassis containing a NI 9234 Sound and Vibration module to capture the acoustic signal from the microphone and a NI 9215 Analogue Voltage Input module to capture the current, voltage and gas flow rate signals. All of these signals were synchronised, captured and stored using software developed in National Instruments Labview. The sampling rates were 51.2 kHz for the acoustic signal and 3 kHz for the current, voltage and gas flow rate signals respectively.

In addition to the recoded welding signals, synchronised high speed video footage was also obtained in order to confirm that the welding tests were producing the expected transfer modes. This footage was recorded using a Basler Ace 640-750um USB camera recording at 2000 fps. In combination with the camera, two 660 nm bandpass filters and a 1.5 neutral density filter were used to attenuate the light emitted by the ignition of the welding arc.

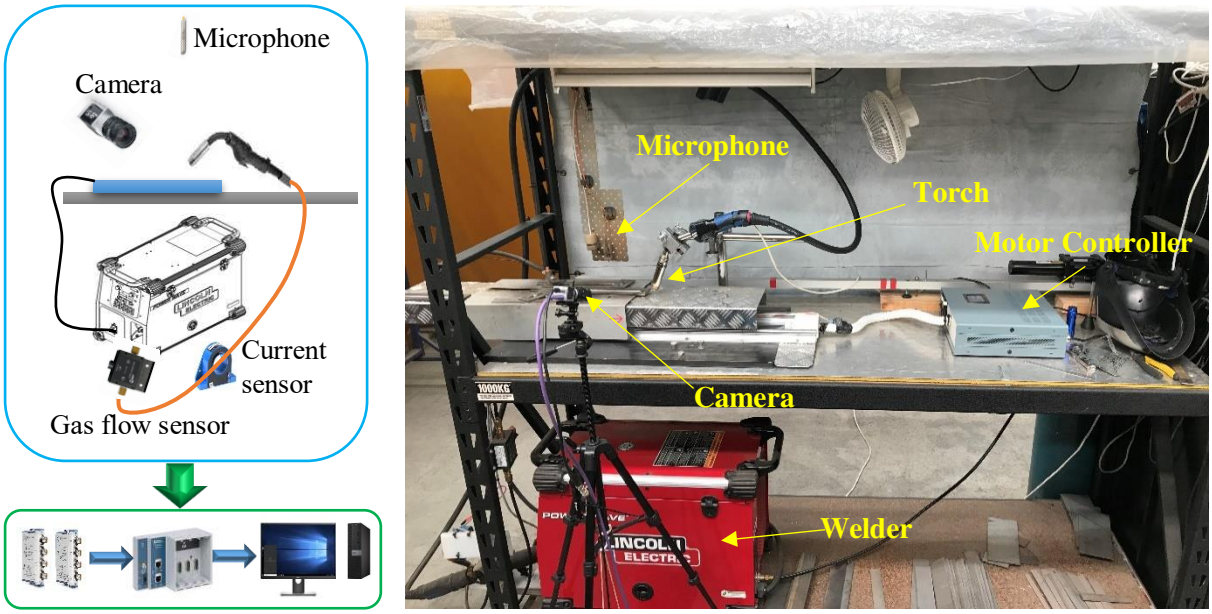

Fig. 1. (a) Diagram and (b) photo of the experimental setup for the measurement system

2.2 Measured multi-sensory signals

To explore the differences between the GMAW transfer modes, 12 individual welds were performed using a range of input values for the Contact Tip to Workpiece Distance (CTWD), travel speed, wire feed rate, voltage and current. The values were chosen in order to reproduce the 5 desired transfer modes, namely, Short Circuit (SC), Free Flight (FF), Pulsed (P), Interchangeable (I) and Explosive (E). The parameters for these welding tests are shown in **Table 1** alongside their corresponding transfer modes.

Table 1 – Welding Parameters

Test Number	Transfer Mode	CTWD (mm)	Travel Speed (mm/min)	Wire Feed Rate (m/min)	Current (A)	Voltage (V)
1	SC	17	230	4.49	93	17.8
2	SC	17	260	5.3	104	19.8
3	SC	14.5	310	6.83	132	19.4
4	E	14.5	260	5.3	101	19.8
5	E	17	310	10	140	28
6	E	15	230	4.52	88	20
7	I	17	370	7.03	131	23.7
8	I	17	370	9.29	140	26
9	FF	18	370	9.8	133	29
10	P	15	420	7.51	113	26.4
11	P	15	420	7.51	118	24
12	P	15	420	7.51	114	27.4

Fig. 2 shows the examples of 100 ms segments of the acoustic, voltage, current, and gas flow rate signals for each of the 5 transfer modes. These signals were recorded with the apparatus given in **Fig. 1** using the parameters outlined in **Table 1**.

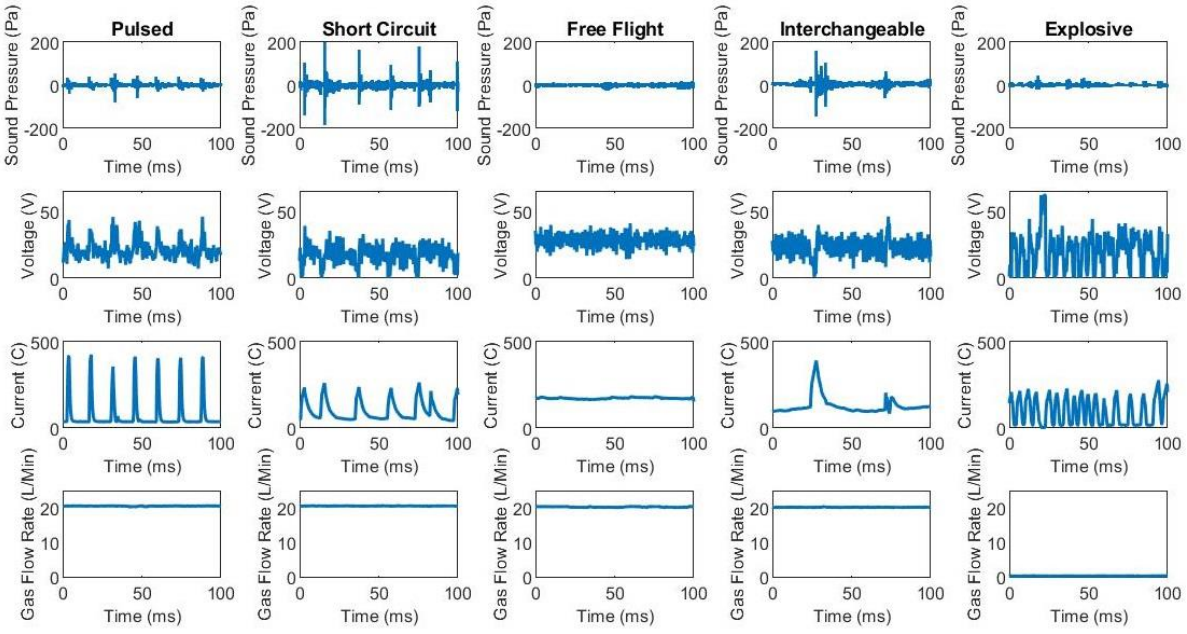

Fig. 2. Comparison of the Sound, Voltage, Current and Gas Flow Rate signals for the 5 GMAW Transfer Mode Classifications

From the signals across the different transfer modes above, it can be seen that there are several differences between the 4 signals. When comparing the acoustic signals it can be observed that there is a distinct difference in the shape and frequency of the signal peaks. In particular, the pulsed, short circuit and interchangeable transfer modes all have distinct peaks in the signal, whereas the free flight and explosive transfer modes are significantly flatter with peaks that are difficult to distinguish from the time domain waveforms. It can also be observed that the short circuit and interchangeable transfer modes display louder sound pulses when compared to the other three transfer modes. This larger sound pulse can be attributed to the high energy arc ignition that occurs when the molten electrode bridge is broken during short circuiting.

When examining the current signal, several differences in the shape of the signal can also be observed. Pulsed, short circuit and interchangeable transfer modes all display very distinct current peaks, while still displaying key differences between the three. Pulsed Transfer mode displays very sharp narrow peaks with a large amplitude that falls back down to a low base current value. Short circuit and interchangeable transfer modes both show shorter, wider peaks while dropping down to a lower base current with Interchangeable transfer mode's base current value being much higher than short circuit and pulsed. This occurs due to the short circuiting of the welding electrode that occurs in both short circuit and interchangeable transfer modes [23]. In contrast, free flight transfer mode demonstrates a flatter signal with less obvious peaks while being at a significantly higher current value when compared to the other signals. In addition, explosive transfer mode demonstrates a much more erratic signal with many pulses varying across several different current values.

In comparison to the acoustic and current signals, the voltage and gas flow rate signals display a less obvious distinction between the 5 transfer modes. For the voltage signals it can be seen that there are increased voltage peaks in the Pulsed transfer mode corresponding to the peaks in the acoustic and current signals. In addition, there are also valleys demonstrating drops in voltage in the short circuit and interchangeable transfer modes corresponding to the short circuiting of the system. Similar to the current signal, the free flight transfer mode displays less obvious peaks and is flatter than the other signals. Explosive transfer mode however, is much more distinguishable with the voltage and gas

signals when compared to the other transfer modes, with the voltage signal being substantially more unstable as well as having zero gas flow rate. This is due to the gas flow being absent in this transfer mode which is evidenced by the zero flow rate shown in **Fig. 2**.

3. Analysis of Transfer Mode Features

3.1 Feature extraction

In order to analyse the acoustic, current, voltage and gas flow rate signals, several time and frequency domain features are extracted, which are summarised in Appendix 1. Several of these features have been used previously to analyse the acoustic signal of the welding process. Zhao et al. [22] used the acoustic features in Eq. (A1-A11) and Eq. (A12-A17) to detect the welding transfer modes and the peak detection analysis seen below in Section 3.2. The Number of Peaks (NP) and Average Peak Height (AP) features are based on the investigation into the shape and frequency of the acoustic signal peaks between different transfer modes conducted by Zhao et al. [17]. In addition to these, Mel Frequency Cepstral Coefficients (MFCC) are also being used as a feature and have been previously used by Zhang et al. [24] to detect defects in GTAW.

MFCC are a common feature used in speech recognition algorithms and are used to distinguish phonemes in speech. MFCC's aim to calculate the energy present between two frequency bands in an audio signal. However due to the human ear's limited ability to detect small frequency changes at higher frequencies, a non-linear Mel scale is used in order to better represent the frequency bands for which the features are calculated. The equation to transform this regular frequency into Mel frequencies can be seen below. [25]

$$M(f) = 1125 \ln\left(1 + \frac{f}{700}\right) \quad (1)$$

As it is well known that professional welders can tell the difference between transfer modes using only the sound signal [18], the use of MFCC's as a feature is both reasonable and appropriate in replicating the ability that professional welders possess.

In order to calculate the number of peaks and average peak height features listed in Appendix 1, the peaks of the recorded signals need to first be obtained. As documented by Zhao et al. [17], the frequency and amplitude of the signal peaks varies between the different transfer modes, hence the two features mentioned above are supposed to act as a decent indicator of the current transfer mode of the system.

To analyse the appearance frequency and shape of the signal peaks, a peak detection algorithm is used to automatically detect the peaks in the signal that correspond to the welding droplet transfers. To detect and calculate the peaks of the signal, the signal envelope of the absolute value of the signal is estimated first then the peaks are calculated by finding x_n points where

$$x_{n-1} < x_n \text{ and } x_n > x_{n+1} \tag{2}$$

After finding all the peaks in the envelope signal, the next step is to analyse the peaks and determine which of the peaks correspond to a single droplet transfer. In order to do this, thresholds need to be set to properly filter out the false peaks in the signal. However, these thresholds need to be relative to each individual signal as an absolute value cannot be determined due to the amplitude differences between different transfer modes. To overcome this difficulty, a two-threshold strategy is used to remove these false peaks, where a threshold is set for both the peak prominence (M_{PP}) and the peak amplitude (M_{PA}). Trial and error shows that the thresholds of $0.5\times M_{PA}$ and $0.2\times M_{PP}$ are optimal to filter out the false peaks. As an example, **Fig. 3a** and **Fig. 3b** show the absolute value of the acoustic signal (upper panels) and the signal envelope (lower panels) with the detected peaks (red circles) of a 20 ms period for the short circuit and free flight transfer modes, respectively. It can be seen that only one distinct pulse is detected in the short circuit transfer mode in comparison to the free flight transfer mode which registers several peaks within the same time period.

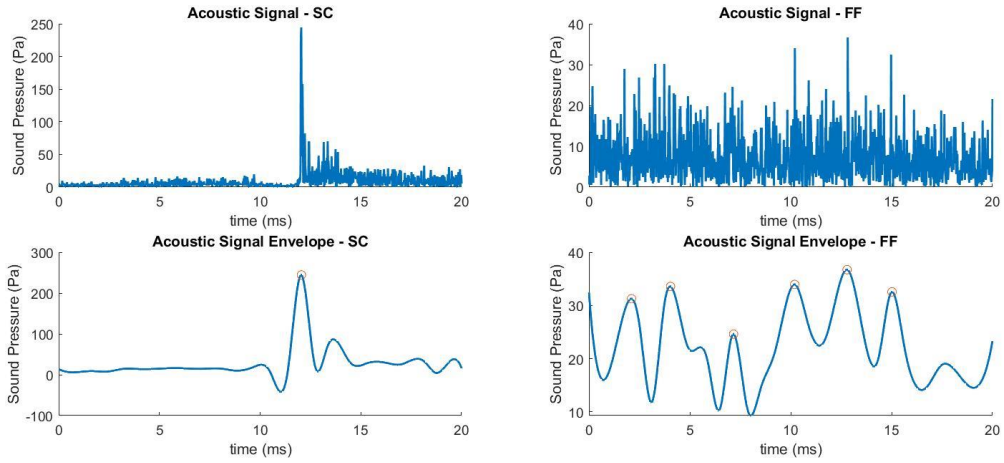

(a) (b)

Fig. 3. Peak Detection of (a) Short Circuit and (b) Free Flight Transfer

3.2 Feature Selection

To reduce the redundant information in the feature set and choose the most appropriate features, a feature selection method is introduced to maximise the distance between each classes' multivariate probability distribution. This distance between each class can be calculated using the Bhattacharyya distance formula [26] below in Eqs. (3) and (4).

$$D_{\mathrm{B}} = \frac{1}{8}\left(\mu_i - \mu_j\right)^T \Sigma^{-1}\left(\mu_i - \mu_j\right) + \frac{1}{2}\ln\left(\frac{det\Sigma}{\sqrt{det\Sigma_i + det\Sigma_j}}\right) \tag{3}$$

$$\Sigma = \frac{\Sigma_i + \Sigma_j}{2} \tag{4}$$

Where μ_i and μ_j and Σ_i and Σ_j are the mean and covariance matrices for the *i*-th and *j*-th multivariate probability distributions, respectively

As the Bhattacharya distance (D_{B}) can only calculate the distance between two classes, all possible combinations between are calculated to achieve a distance that is representative of all the classes. Using all combinations of D_{B}, a new weighted distance classifier, *C*, is calculated to represent the overall viability that the feature set has at maximising the distance between all of the classes. This C value is calculated from Eqs. (5-7), where D_{min} and D_{avg} are the minimum and average values of D_{B}

for all class combinations, respectively, M is the number of classes, and μ is mean matrix consisting of k number of features.

$$D_{\min} = \min(D_{\mathrm{B}}(i,j) \mid i \in \{1,\dots,M\}, j \in \{i+1,\dots,M\}) \tag{5}$$

$$D_{\mathrm{avg}} = \frac{2!\,(M-2)!}{M!}\sum_{i=1}^{M}\sum_{j=i+1}^{M} D_{\mathrm{B}}(i,j) \tag{6}$$

$$C = \frac{\left(D_{\min} + D_{\mathrm{avg}}\right)}{\sqrt{k}} \tag{7}$$

The C value calculated above takes into account both $D_{\min}$ and D_{avg} in order to make sure that the average value of D_{B} can be maximised while still making sure that each class combination maintains a maximum distance between each other. $D_{\min}$ and D_{avg} are then divided by $\sqrt{k}$ to normalise the value of C as the length of the feature set used to calculate D_{B} grows.

To obtain the optimal set of features R_n from the initial feature set F, a modified version of the Sequential Forward Floating Selection (SFFS) algorithm which was originally implemented by García-Allende et al. [26] is developed. This algorithm selects one feature from the initial feature set first, and then adds additional features to the set that maximises the value of C. Whenever the algorithm adds a feature to the feature set, it also tests to see if removing any of the features from the feature set can further maximise the value of C. This process is repeated until such a point where both adding or removing features no longer increases the value of C. This algorithm is schematically illustrated in **Fig. 4** which shows the process to select the optimal feature set, where f is a feature of the original feature set F, f_{add} is the feature that is added to R_n that maximises the value of C, f_{sub} is the feature that is subtracted from R_n that maximises the value of C, and n is the number of features in the final feature set R_n.

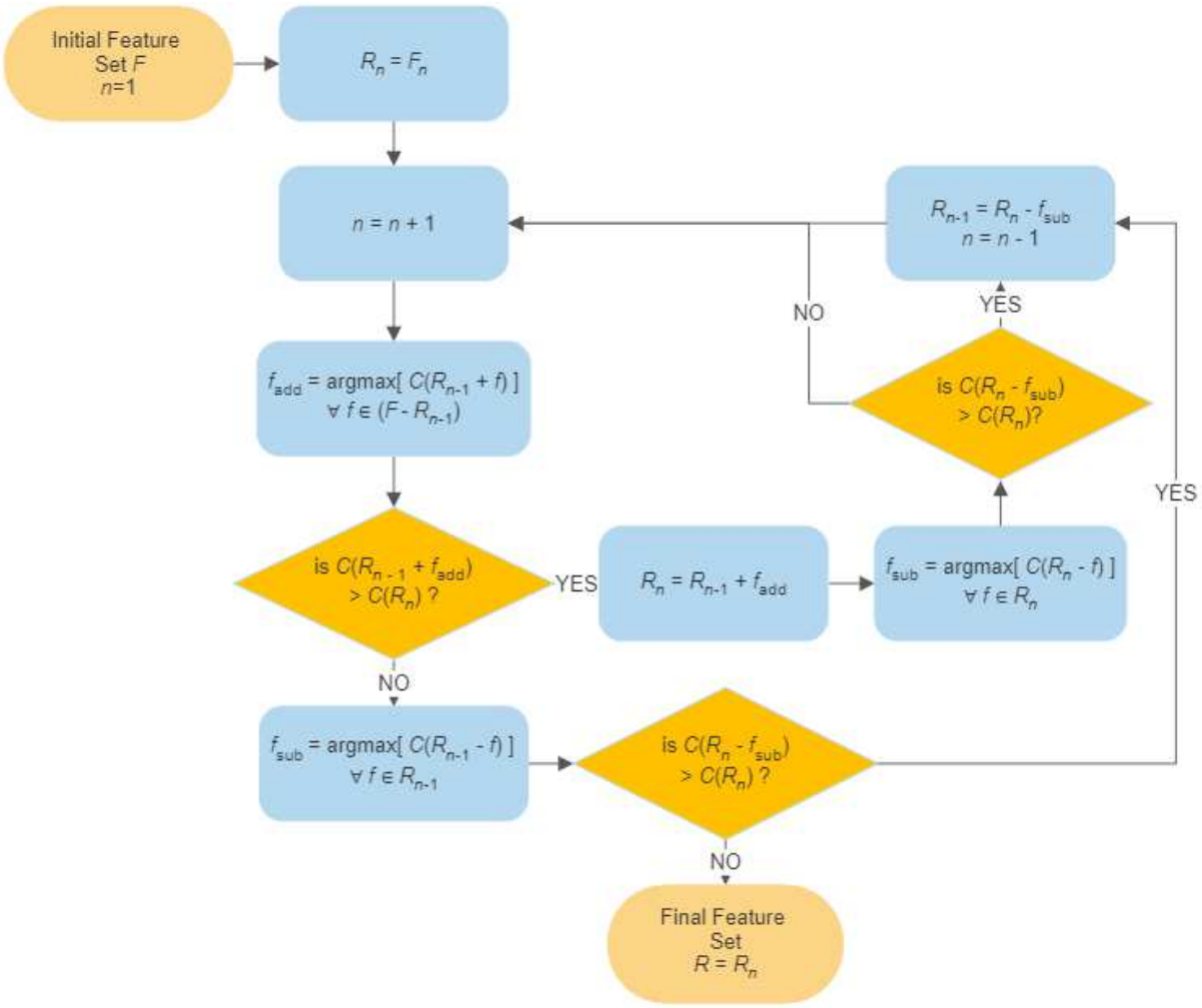

Fig. 4. Diagram of the Feature Selection Algorithm

3.3 SVM classifier training and testing

The SVM is used as the classifier for the automatic metal transfer mode classification system because it is simple and easy to implement in a portable system. The SVM classifiers use a Radial Basis Function (RBF) kernel and are trained with the features selected by the feature selection algorithm which are then normalised.

To create a large enough database of signals to train the SVM classifiers, each of the 12 recorded signals shown in

Table **1** – Welding Parameters are divided into smaller segment lengths. Ideally, the optimum length of these smaller segments would be as short as possible without sacrificing the prediction accuracy of the SVM classifiers because it would allow for less individual droplet transfers being analysed in each segment. Therefore 5 different segment lengths are chosen to train the SVM classifier in order to investigate the prediction accuracy as the segment lengths become shorter. These segment lengths are 100 ms, 50 ms, 40 ms, 30 ms, and 20 ms, respectively.

Using the database of smaller signal segments, the optimal features are extracted for each segment and are then used to train the SVM classifiers. A total of 5 tests are performed in the experiments. The SVM classifier is first trained using the features obtained from the individual acoustic, current, voltage, and gas flow rate signal segments, respectively. Then the combined features obtained from all the four base signals are used to train the SVM classifier. This process is then repeated 5 times using each of the 5 different segment lengths.

In order to test the prediction accuracy, each SVM classifier is subjected to 10-fold cross validation. The training data set is randomly divided into 10 equal sets, 9 of which are used to train the SVM classifier while the 10^{th} set is used to test the accuracy. This is repeated again until all 10 sets have been used to train and test the model, and the accuracy for each set are averaged to produce a prediction rate.

4. Results and Discussions

4.1 Feature selection results

The feature selection algorithm is able to effectively reduce the dimensionality of the original feature set while only retaining the optimal features for class separability. In the experiment, the desired features, which maximise the value of C, are selected from the original feature set F. As an example, **Table 2** shows the features selected by the feature selection algorithm using only the acoustic signals across the 5 different segment lengths.

Table 2 – Common Acoustic only Method Features

Features	Signal segment length				
	100 ms	50 ms	40 ms	30 ms	20 ms
Zero Crossing Rate (ZCR)	Y	Y	Y	Y	Y
Root Mean Square (RMS)	Y	Y	Y	Y	Y
Square root of amplitude (SRA)	Y	Y	Y	Y	Y
Kurtosis Value (K)	Y	Y	Y	Y	Y
Skewness value (S)	Y	Y	Y	Y	Y
Peak to Peak Value (P2P)	Y	Y	Y	Y	Y
Crest Factor (CF)	Y	Y	Y	Y	Y
Impulse Factor (IF)	Y	Y	Y	Y	Y
Margin Factor (MF)	Y	Y	Y	Y	Y
Shape Factor (SF)	Y	Y	Y	Y	Y
Peak Frequency (PF)	Y	Y	N	N	N
Frequency centre (FC)	N	N	N	N	N
Root Mean Square Frequency (RMSF)	N	N	N	N	N
Root Variance Frequency (RVF)	N	N	N	N	N
Number of Peaks (NP)	Y	Y	Y	N	N
Average Peak Height (AP)	Y	Y	Y	Y	Y
Signal Average (SA)	Y	Y	Y	Y	Y
Max Frequency (FM)	Y	Y	Y	Y	Y
Average Frequency (FA)	Y	Y	Y	Y	Y
MFCC log energy	Y	Y	Y	Y	Y
MFCC band 0-500hz	Y	Y	Y	Y	Y
MFCC band 200-850hz	Y	Y	Y	Y	Y
MFCC band 500-1300hz	Y	Y	Y	Y	Y
MFCC band 850-1900hz	Y	Y	Y	Y	Y
MFCC band 1300-2650hz	Y	Y	Y	Y	Y
MFCC band 1900-3650hz	N	N	N	N	N
MFCC band 2650-4900hz	N	N	N	N	N
MFCC band 3650-6550hz	N	N	N	N	N
MFCC band 4900-8700hz	N	N	N	N	N
MFCC band 6550-11450hz	N	N	N	N	N
MFCC band 8700-15000hz	N	N	N	N	N
MFCC band 11450-19650hz	N	N	N	N	N
MFCC band 15000-25600hz	N	N	N	N	N

From **Table 2** it can be observed that approximately a third of the features (on average 13 out of 33) from the original feature set are excluded by the feature selection algorithm. It can also be seen that while majority of the features selected by the algorithm are identical among the 5 segment length tests, both the NP and PF features were selected in only the longer segment lengths tests. This leads to some of the selected features being situationally useful, where they only show a large amount of class separability at either short or long segment lengths. The features selected by the algorithm in the 20 ms test can be seen below in **Fig. 5**, which shows the mean values of each feature for each of the 5

transfer mode. The results for other segment lengths (30 ms, 40 ms, 50 ms and 100 ms) and other signals (current, voltage and gas flow rate) are similar and not shown here for the sake of brevity.

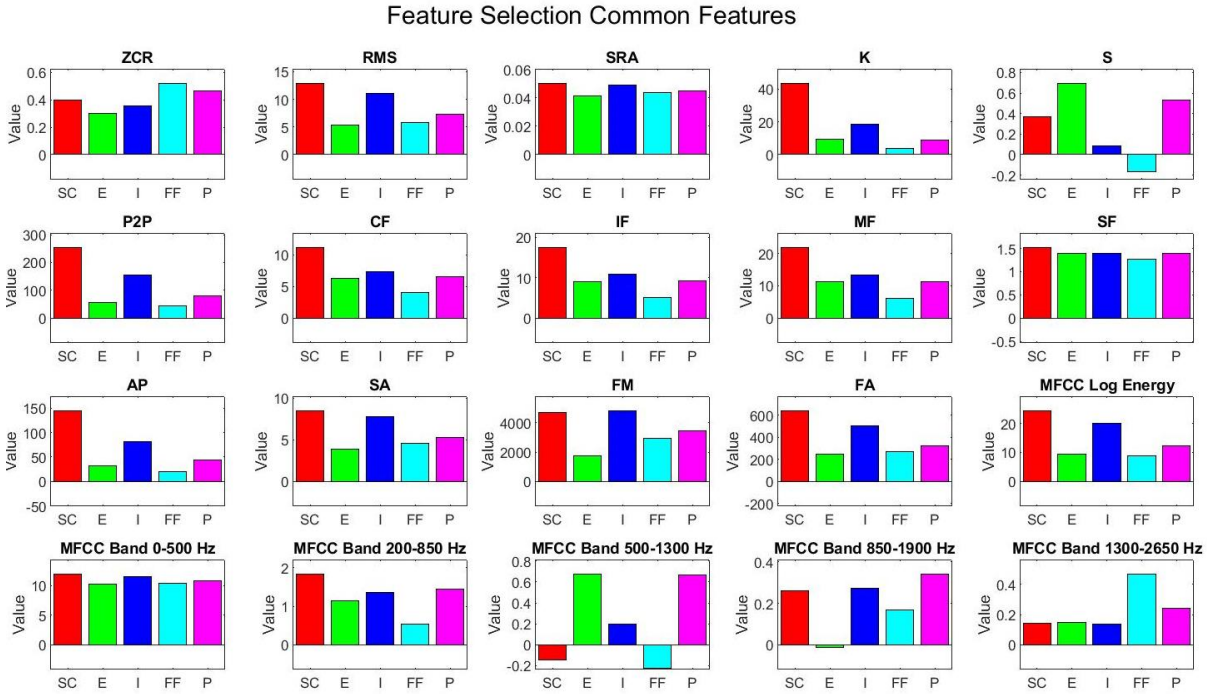

Fig. 5. Mean values of Acoustic Features selected by the feature selection algorithm for 20 ms segments.

Fig. 5 shows that each individual feature selected by the algorithm cannot effectively separate all 5 classes on its own. However, the feature selection algorithm successfully chooses a combination of features that are able to maximise the distance between each of the individual classes. For example, when looking at the explosive transfer (Green Bar) and pulsed transfer (Purple Bar) values in majority of the common features shown in **Fig. 5**, it can be seen that the mean values are shown to be very similar. However, due to the class separability value, *C* shown in Eq. (7), the feature selection algorithm selects features to address this issue such as MFCC Band 850-1900 Hz, which shows a large degree of separability between explosive and free flight transfer modes. This can be better understood when observing the values of the class separability value, *C* at each iteration of the feature selection algorithm as shown below in **Fig. 6**.

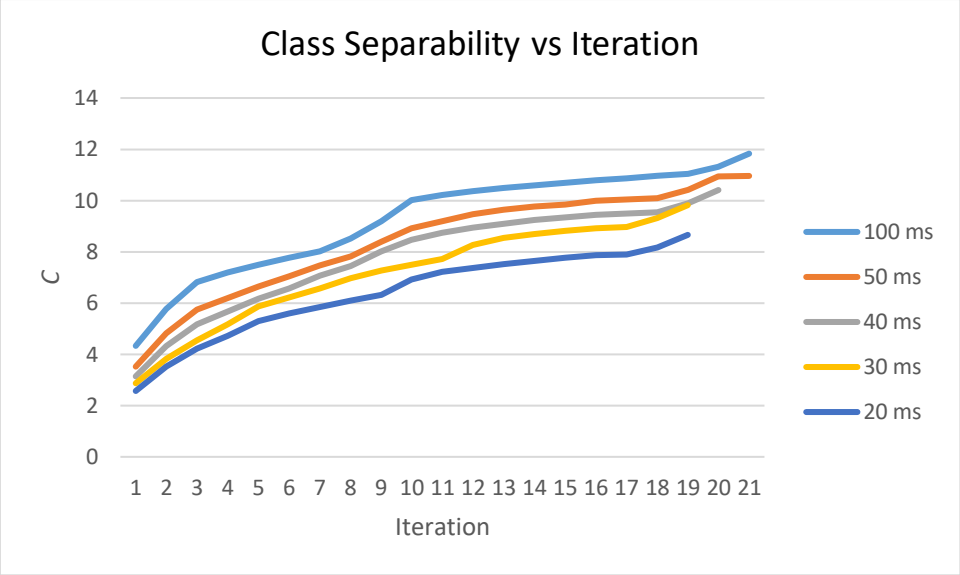

Fig. 6. Class separability value *C* at each iteration of the feature selection algorithm for the acoustic only method

The class separability values in **Fig. 6** show that as additional features are added and removed at each iteration of the feature selection process, the overall value of the class separability is increased. At iteration 1 of the feature selection algorithm, the 2 features with the highest class separability value are selected. The results displayed in **Fig. 6** however show that the value of *C* for the feature set selected at iteration 1 can be improved by upwards of 300% when more features are added, reaching a maximum class separation value at its final iteration. For comparison, the values of *C* for the original feature set alongside the final *C* values when using the feature selection algorithm as well as the values for the excluded features are summarised below in **Table 3**.

Table 3 – Class Separability value *C* for the feature selection and original feature sets

Feature Set	Segment Length				
	100 ms	50 ms	40 ms	30 ms	20 ms
Unselected Features	2.33	1.97	1.67	1.49	1.15
Original	11.37	10.18	9.54	8.92	7.72
Feature Selection	11.83	10.96	10.41	9.82	8.66

Observing the results above in **Table 3** it can be seen that the feature selection algorithm is able to effectively increase the value of *C* when compared to the value obtained using the original feature set. As stated above in the feature selection algorithm section, a higher class separability value *C* corresponds to a larger average separation distance between the 5 different classes. This increase in value is also shown to be much larger in the shorter segment length tests than it is in the longer segment length tests, suggesting that many of the features that the feature reduction algorithm excludes have a larger negative impact on the class separability at shorter segment lengths.

4.2 Classification results

As outlined in Section 3, five tests were performed and repeated across 5 different segment lengths. The first 4 tests used feature sets from either the acoustic, current, voltage or gas flow rate signals individually while the final test used a combined feature set consisting of the features from all the 4 signals. When the original feature set is used (without the feature selection algorithm), the 10-fold cross validation results are shown in **Table 4**. It can be seen that the SVM classifier was able to achieve a level of accuracy greater than 80% across the five tests. Both the gas flow rate and current only methods show the highest accuracies being approximately 85% accurate with the acoustic, voltage and combined methods being slightly less accurate with prediction accuracies of approximately 80%.

Table 4 – SVM accuracy results (Original Feature Set)

Segment Length	Accuracy (%)				
	Acoustic features only	Current features only	Voltage features only	Gas features only	Combined features
100 ms	81.12	86.59	81.72	87.24	80.00
50 ms	81.21	86.49	81.61	85.64	80.00
40 ms	81.26	85.80	81.61	85.15	80.00
30 ms	81.24	85.75	81.35	84.86	80.00
20 ms	81.22	86.06	81.43	83.54	79.89

Similarly, the 10-fold cross validation of the SVM classifiers trained using the feature sets selected by the feature selection algorithm are summarised in **Table 5**. By comparing **Table 4** and **Table 5**, it can be observed that the application of the feature selection algorithm leads to significantly higher prediction accuracies across the acoustic, current, voltage, and combined methods. On average the inclusion of the feature selection algorithm improved the classification accuracies by approximately 15% when compared to the results shown in **Table 4**.

Table 5 – SVM Classifier Accuracy Results (Feature Selection)

Segment Length	Accuracy (%)				
	Acoustic features only	Current features only	Voltage features only	Gas features only	Combined features
100 ms	96.49	99.31	99.86	84.63	99.74
50 ms	96.25	99.13	99.61	86.26	99.72
40 ms	96.65	98.94	99.49	87.48	99.75
30 ms	96.88	97.76	99.43	87.20	99.74
20 ms	96.76	97.52	98.54	87.17	99.76

When comparing the classification accuracies among the 5 methods in **Table 5** it can be seen that the combined signal method produced the highest level of accuracy with an average prediction accuracy of greater than 99.7% across the 5 different segment length trials. This was expected as the feature reduction algorithm uses all features calculated from the 4 signals and chooses the best feature set accordingly. In addition to the combined signal method, the accuracies of the Acoustic, Current and Voltage only methods all were able to achieve a prediction accuracy of 96%, 98%, 99% respectively. When comparing these methods to the combined method it can be seen that there is only a minor drop in accuracy. This is especially the case for the current and voltage methods which have an average accuracy of only 2% lower than the combined mode. Despite the presence of loud background noise

in the factory, the achieved prediction accuracy is as high as 96.8% when the SVM classifier is trained with the acoustic signal only, which is promising for practical applications with the advantage of non-intrusiveness and portability. The accuracy of acoustic signal only prediction can be further improved in the future, by utilizing various beamforming algorithms based on a microphone array to enhance the welding sound signal from other noises and increase the robustness of the acoustic sensing based approach.

It should be noted that when the gas flow rate is used as the individual signals for the SVM classifier, it is significantly less accurate than the other methods once the feature selection algorithm is applied. This is reasonable as the gas flow rate is incredibly similar between 4 of the 5 transfer mode classes with only the explosive transfer mode with no shielding gas. The higher accuracy of this method when the feature selection algorithm is not used compared to the other tests in **Table 4** may be the result of overfitting due to the gas flow rate having an almost constant value throughout each of the 12 original signals.

Both **Table 4** and **Table 5** show that the accuracies remained relatively similar across the 5 different segment lengths in both the acoustic only and combined signal trials, demonstrating the feasibility of real-time process monitoring within a time window as short as 20 ms. This can also provide instant feedback information on welding quality, enabling adaptive real-time control of weld parameters for fully automated welding robotics.

4.3 Discussions

When analysing the results for both the acoustic and the combined tests, it was found that the model may not provide a good identification when trying to classify the interchangeable transfer modes correctly. In particular, the model's minimum prediction results occur when classifying interchangeable transfer modes as short circuit transfer modes in the acoustic only method. This can be observed in **Table 6** which shows the classification accuracies for the acoustic only test, broken down into the individual transfer mode accuracy predictions.

Table 6 – Acoustic only SVM classification accuracies by transfer modes

Signal Length	Short-circuit	Explosive	Interchangeable	Free-flight	Pulsed
100 ms	95.40	99.08	90.90	98.50	98.54
50 ms	95.02	98.44	90.46	98.84	98.51
40 ms	95.08	98.54	91.67	99.23	98.73
30 ms	95.06	98.80	92.26	99.52	98.78
20 ms	94.83	98.47	92.32	99.41	98.76

Below are two examples that can help explain this phenomenon. **Fig. 7** and **Fig. 8** show the acoustic, voltage, current and the high speed video signals of an interchangeable and short circuit transfer mode with a 20 ms segment length respectively.

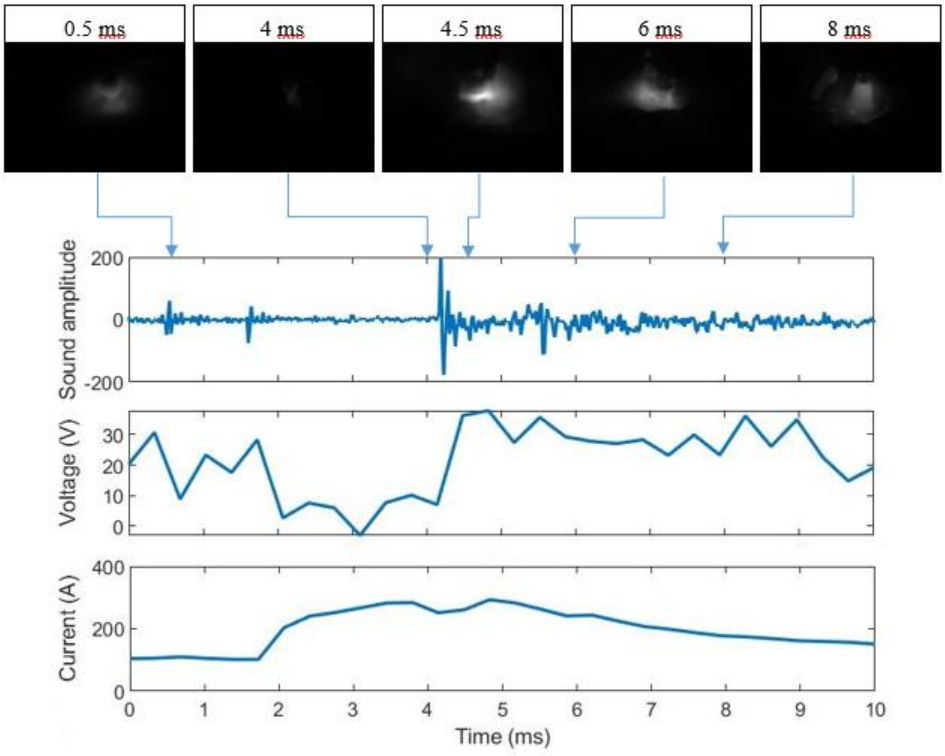

Fig. 7. Interchangeable Transfer Mode Signal

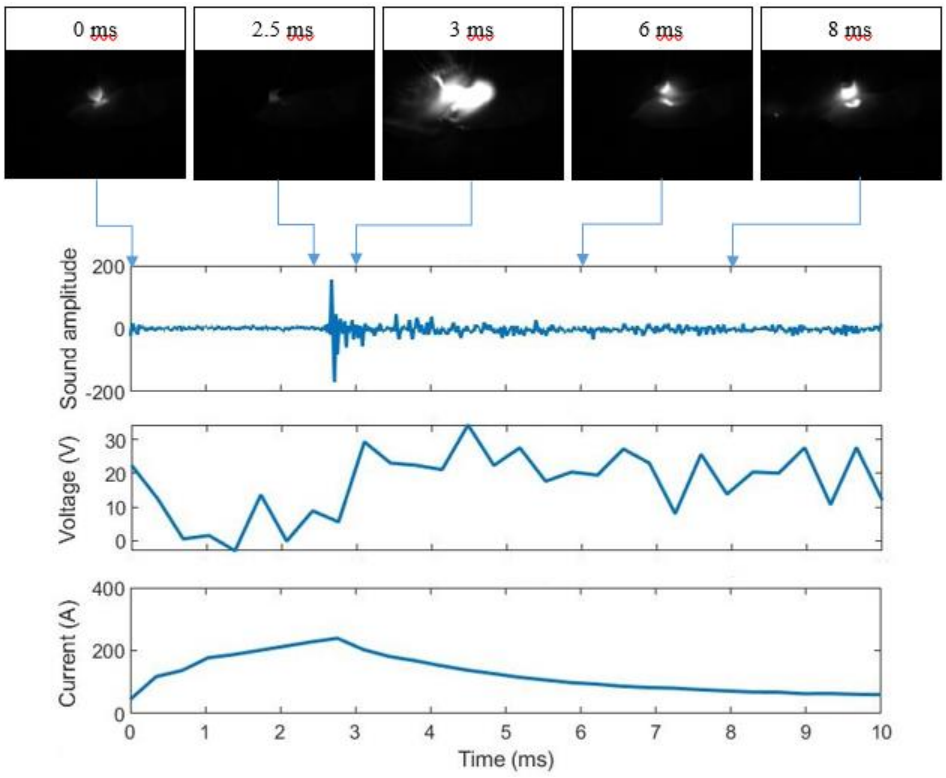

Fig. 8. Interchangeable Transfer Mode Signal

The acoustic signals in both of the above figures depict that they both look very similar with one distinct peak which heavily represents a short circuit transfer. The corresponding video footage of the two different signals illustrate that they both were in fact short circuit transfer modes confirming this observation in the acoustic signal. In addition, the acoustic only SVM classifier also classified both of these signals as short circuit transfer mode, which would show the interchangeable transfer mode as being an incorrect prediction in the results.

On the contrary, when observing the combined SVM method results, the SVM was able to correctly identify the interchangeable transfer mode segment in **Fig. 7** despite it looking like a short circuit transfer. This is due to the inclusion of the current and voltage signals which reveal more details about the transfer that the features extracted from the acoustic signal at this stage cannot currently identify. When comparing the two figures, one of the more obvious distinctions between the two which helps differentiate the two is the base level of the current signal before and after the pulse. It can be seen that the base level of the current in **Fig. 7** is higher than that in **Fig. 8**. This higher current fits the

conditions for Globular-Short Circuit- Streaming Spray Interchangeable Mode [6] which is the literature classification of the interchangeable transfer modes that were used in this test.

Taking the observations above into consideration, it may be extremely difficult to distinguish some interchangeable transfer mode segments, especially with shorter segment lengths when only using the acoustic signal. While the system might very well be in an interchangeable transfer mode, the acoustic signal mainly only picks up the sound generated from the detachment of the welding droplet. This does not show any information about the welding parameters which seem to be crucial in analysing the stability of the current transfer mode. As an example, the two signals in **Fig. 7** & **Fig. 8** both realistically show a short circuit transfer. However, when the current and voltage signals are taken into account, the base level current is too high to maintain a stable short circuit transfer mode causing the cyclic behaviour of Globular-Short Circuit-Streaming Spray transfer.

Despite all of this, it may still be beneficial to classify both of the examples in **Fig. 7** and **Fig. 8** as short circuit transfer modes instead of interchangeable transfer modes, especially in the case of shorter segment lengths. As only a single droplet transfer is being captured in a large majority of the shorter segment lengths for short circuit and interchangeable transfer modes, it should technically be classified as short circuit transfer as the transfer mode of the droplet is not actually changing within the individual segment. If a real time classification system is to designed based on this work, the conditions that constitute an interchangeable transfer mode should be based on analysing subsequent recorded segments and if the transfer mode differs between these segments then the system would be in an interchangeable mode. From this perspective, it is more beneficial to use only the acoustic signal to classify the transfer modes, because it is more accurately able to achieve the correct classification based on the actual droplet transfer instead of the shape of the welding parameter signals that cause the process to occur.

5. Conclusion

In this paper, a new GMAW transfer mode classification method has been introduced based on acoustic signal analysis. Five models were created using a combination of time and frequency domain

features extracted from the acoustic, current, voltage and gas flow signals. The time and frequency time features are used to train a SVM classifier for automatic transfer mode detection. A feature selection algorithm is proposed to find the optimal features with minimum redundant information to further improve the prediction accuracy. It was found that, when using only the acoustic signal, the proposed feature selection algorithm improves the prediction accuracy from around 81% to approximate 96%. This is comparable to the prediction accuracy with all the acoustic, current, voltage and gas flow rate signals, which are approximate 99% and 80% with and without using the developed feature selection algorithm, respectively. The high accuracy of the acoustic signal only model shows the most promise due to its non-intrusiveness and the simplicity of the measurement system, which allows it to be easily implemented into a smart welding system. Future work includes further classification between additional transfer modes, in particular differentiation between the different free flight transfer modes. In addition to this, a real time adaptive feedback control system will be developed based off of the transfer mode detection algorithm introduced in this paper.

Acknowledgements

The authors would like to thank Malcolm Rigby and Anthony Lele from Sound Intuition Pty. Ltd. for their permission to use the experimental data in the paper.

Declarations

-Ethics Approval

Not applicable.

-Consent to Participate

The authors consent to participate in the review process

-Consent to Publish

The authors consent to publish this research

-Authors Contributions

Mitchell Cullen - Research, Test Rig Design, Data collection, Data Analysis, Detection Algorithm, Initial Draft

Sipei Zhao - Test Rig Design, Data Collection, Editing

JC Ji - Editing, Advisor

Xiaojun Qiu - Advisor

-Funding

This research was supported under the Australian Research Council's Linkage Project (No. LP160100616) and the UTS FEIT Tech Lab Blue Sky Grant.

-Competing interests

The authors declare that they have no conflict of interest.

-Availability of data and materials

Code and raw data are available upon request.

Appendix

The features extracted from the signals and their definitions are summarised in Table A1.

Table A1 - Time and Frequency Domain Features

Number	Time Domain Features	
1	Zero Crossing Rate (ZCR)	$ZCR = \frac{f_s}{N}\sum_{n=0}^{N-1}\left\lvert sgn\big(x(n)\big) - sgn\big(x(n-1)\big)\right\rvert$ $(A1)$
2	Root mean square (RMS)	$X_{rms} = \left(\frac{1}{N}\sum_{i=1}^{N} x_i^2\right)^{\frac{1}{2}}$ $(A2)$

3	Square root of the amplitude (SRA)	$X_{sra} = \left(\frac{1}{N}\sum_{i=1}^{N}\sqrt{\lvert x_i \rvert}\right)^2$	$(A3)$
4	Kurtosis value (K)	$X_{kv} = \frac{1}{N}\sum_{i=1}^{N}\left(\frac{x_i - \bar{x}}{\sigma}\right)^4$	$(A4)$
5	Skewness value (S)	$X_{sv} = \frac{1}{N}\sum_{i=1}^{N}\left(\frac{x_i - \bar{x}}{\sigma}\right)^3$	$(A5)$
6	Peak-peak value (P2P)	$X_{ppv} = \max(x_i) - \min(x_i)$	$(A6)$
7	Crest factor (CF)	$X_{cf} = \max(\lvert x_i \rvert) \Big/ \left(\frac{1}{N}\sum_{i=1}^{N} x_i^2\right)^{\frac{1}{2}}$	$(A7)$
8	Impulse factor (IF)	$X_{if} = \max(\lvert x_i \rvert) \Big/ \frac{1}{N}\sum_{i=1}^{N}\lvert x_i \rvert$	$(A8)$
9	Margin factor (MF)	$X_{mf} = \max(\lvert x_i \rvert) \Big/ \left(\frac{1}{N}\sum_{i=1}^{N}\sqrt{\lvert x_i \rvert}\right)^2$	$(A9)$
10	Shape factor (SF)	$X_{sf} = \left(\frac{1}{N}\sum_{i=1}^{N} x_i^2\right)^{\frac{1}{2}} \Big/ \frac{1}{N}\sum_{i=1}^{N}\lvert x_i \rvert$	$(A10)$
11	Number of Peaks (NP)	(see section 3.2)	
12	Average Peak Height (AP)	(see section 3.2)	
13	Signal Average (SA)	$X_{avg} = \frac{1}{N}\sum_{i=1}^{N}\lvert x_i \rvert$	$(A11)$
Frequency Domain Features			
14	Peak frequency (PF)	$maxarg\big(s(f)\big)$	$(A12)$

15	Frequency centre (FC)	$X_{fc} = \int_0^{+\infty} fs(f)df \Big/ \int_0^{+\infty} s(f)df$	(A13)
16	RMS frequency (RMSF)	$X_{rmsf} = \left(\int_0^{+\infty} f^2 s(f)df \Big/ \int_0^{+\infty} s(f)df \right)^{\frac{1}{2}}$	(A14)
17	Root variance frequency (RVF)	$X_{rvf} = \left(\int_0^{+\infty} (f - X_{fc})^2 s(f)df \Big/ \int_0^{+\infty} s(f)df \right)^{\frac{1}{2}}$	(A15)
18	Max Frequency (FM)	$\max(s(f))$	(A16)
19	Average Frequency (FA)	$AF = \frac{1}{N} \sum_{i=1}^{N} s(f)_i$	(A17)
20	MFCC	(see section 3.3)	

References

1. Scotti A, Ponomarev V, Lucas W (2012) A scientific application oriented classification for metal transfer modes in GMA welding. Journal of Materials Processing Technology 212 (6):1406-1413. doi:https://doi.org/10.1016/j.jmatprotec.2012.01.021

2. Kah P, Latifi H, Suoranta R, Martikainen J, Pirinen M (2014) Usability of arc types in industrial welding. International Journal of Mechanical and Materials Engineering 9:1-12. doi:10.1186/s40712-014-0015-6

3. Lancaster JF (1986) Metal Transfer and Mass Flow in the Weld Pool. In: Lancaster JF (ed) The Physics of Welding (Second Edition). Pergamon Press, Oxford, pp 228-305. doi:https://doi.org/10.1016/B978-0-08-034076-0.50014-1

4. Kim YS, Eager TW (1993) Analysis of metal transfer in gas metal arc welding. Welding Journal 72:269-278

5. Iordachescu D, Quintino L (2008) Steps toward a new classification of metal transfer in gas metal arc welding. Journal of Materials Processing Technology 202 (1):391-397. doi:https://doi.org/10.1016/j.jmatprotec.2007.08.081

6. Scotti A, Ponomarev V, Lucas W (2014) Interchangeable metal transfer phenomenon in GMA welding: Features, mechanisms, classification. Journal of Materials Processing Technology 214 (11):2488-2496. doi:https://doi.org/10.1016/j.jmatprotec.2014.05.022

7. Matteson A, Morris R, Tate R Real-time GMAW quality classification using an artificial neural network with airborne acoustic signals as inputs. In: Salama MMT, Masao Liu, S. Dos Santos, J.F.

Kocak, M. Williams, J. (ed) OMAE `93: 12th international conference on offshore mechanics and arctic engineering, Glasgow, United Kingdom, 1993. pp 20-24

8. Tam J, Huissoon JP Developing psycho-acoustic experiments in gas metal arc welding. In: Gu J, Liu PX (eds) International Conference on Mechatronics & Automation, Niagara Falls, Canada, 2005. pp 1112-1117 Vol. 1112. doi:10.1109/ICMA.2005.1626707

9. Zhao S, Qiu X, Burnett I, Rigby M, Lele A (2021) A lumped-parameter model for sound generation in gas metal arc welding. Mechanical Systems and Signal Processing 147. doi:https://doi.org/10.1016/j.ymssp.2020.107085

10. Jolly WD (1969) Acoustic Emission Exposes Cracks during Welding. The Welding Journal 48:21-27

11. Carlson NM, Johnson JA, Smartt HB (1990) Sensing of Metal-Transfer Mode for Process Control of GMAW. Review of Progress in Quantitative Nondestructive Evaluation 9:1965-1972

12. Saini D, Floyd S (1998) An investigation of gas metal arc welding sound signature for on-line quality control. Welding Research Supplement:172-179

13. Grad L, Grum J, Polajnar I, Marko Slabe J (2004) Feasibility study of acoustic signals for on-line monitoring in short circuit gas metal arc welding. International Journal of Machine Tools and Manufacture 44 (5):555-561. doi:https://doi.org/10.1016/j.ijmachtools.2003.10.016

14. Cayo EH, Alfaro SCA (2009) A Non-Intrusive GMA Welding Process Quality Monitoring System Using Acoustic Sensing. Sensors (Basel) 9 (9):7150-7166. doi:10.3390/s90907150

15. Zhang L, Basantes-Defaz AC, Ozevin D, Indacochea E (2019) Real-time monitoring of welding process using air-coupled ultrasonics and acoustic emission. The International Journal of Advanced Manufacturing Technology 101 (5):1623-1634. doi:10.1007/s00170-018-3042-2

16. Chen C, Xiao R, Chen H, Lv N, Chen S (2020) Arc sound model for pulsed GTAW and recognition of different penetration states. The International Journal of Advanced Manufacturing Technology 108 (9-10):3175-3191. doi:http://dx.doi.org/10.1007/s00170-020-05462-z

17. Zhao S, Qiu X, Burnett I, Rigby M, Lele A Statistical characteristics of Gas Metal Arc Welding (GMAW) sound. In: Ochmann M, Vorländer M, Fels J (eds) 23rd International Congress on Acoustics, Aachen, Germany, 2020. pp 7594-7601. doi:10.13140/RG.2.2.31782.55366

18. Tam J (2005) Methods of Characterizing Gas-Metal Arc Welding Acoustics for Process Automation. University of Waterloo,

19. Wang J, Huissoon JP Classifying Arc Acoustic Data in GMA Welding Using Artificial Neural Network and Naïve Bayesian Classifiers. In: David SA, DebRoy T, DuPont JN, Koseki JN, Smartt HB (eds) Trends in Welding Research, Georgia, USA, 01/01 2008. pp 461-466. doi:10.1361/cp2008twr461

20. Rudas JS, Restrepo JS, Gómez LM Prediction of metal transfer modes in the GMAW process. In: 2015 IEEE 2nd Colombian Conference on Automatic Control (CCAC), 14-16 Oct. 2015 2015. pp 1-6. doi:10.1109/CCAC.2015.7345190

21. Lv N, Xu Y, Li S, Yu X, Chen S (2017) Automated control of welding penetration based on audio sensing technology. Journal of Materials Processing Technology 250:81-98. doi:https://doi.org/10.1016/j.jmatprotec.2017.07.005

22. Zhao S, Qiu X, Burnett I, Rigby M, Lele A GMAW metal transfer mode identification from welding sound. In: Proceedings of ACOUSTICS 2018, Adelaide, Australia, 7-9 November 2018 2018.

23. Wang Y, Lü X, Jing H (2016) Dynamic simulation of short-circuiting transfer in GMAW based on the "mass-spring" model. The International Journal of Advanced Manufacturing Technology 87 (1):897-907. doi:10.1007/s00170-016-8538-z

24. Zhang Z, Wen G, Chen S (2018) Audible Sound-Based Intelligent Evaluation for Aluminum Alloy in Robotic Pulsed GTAW: Mechanism, Feature Selection, and Defect Detection. IEEE Transactions on Industrial Informatics 14 (7):2973-2983. doi:10.1109/TII.2017.2775218

25. Koolagudi SG, Rastogi D, Rao KS (2012) Identification of Language using Mel-Frequency Cepstral Coefficients (MFCC). Procedia Engineering 38:3391-3398. doi:https://doi.org/10.1016/j.proeng.2012.06.392

26. García-Allende PB, Mirapeix J, Conde OM, Cobo A, López-Higuera JM (2009) Spectral processing technique based on feature selection and artificial neural networks for arc-welding quality monitoring. NDT & E International 42 (1):56-63. doi:https://doi.org/10.1016/j.ndteint.2008.07.004

Figures

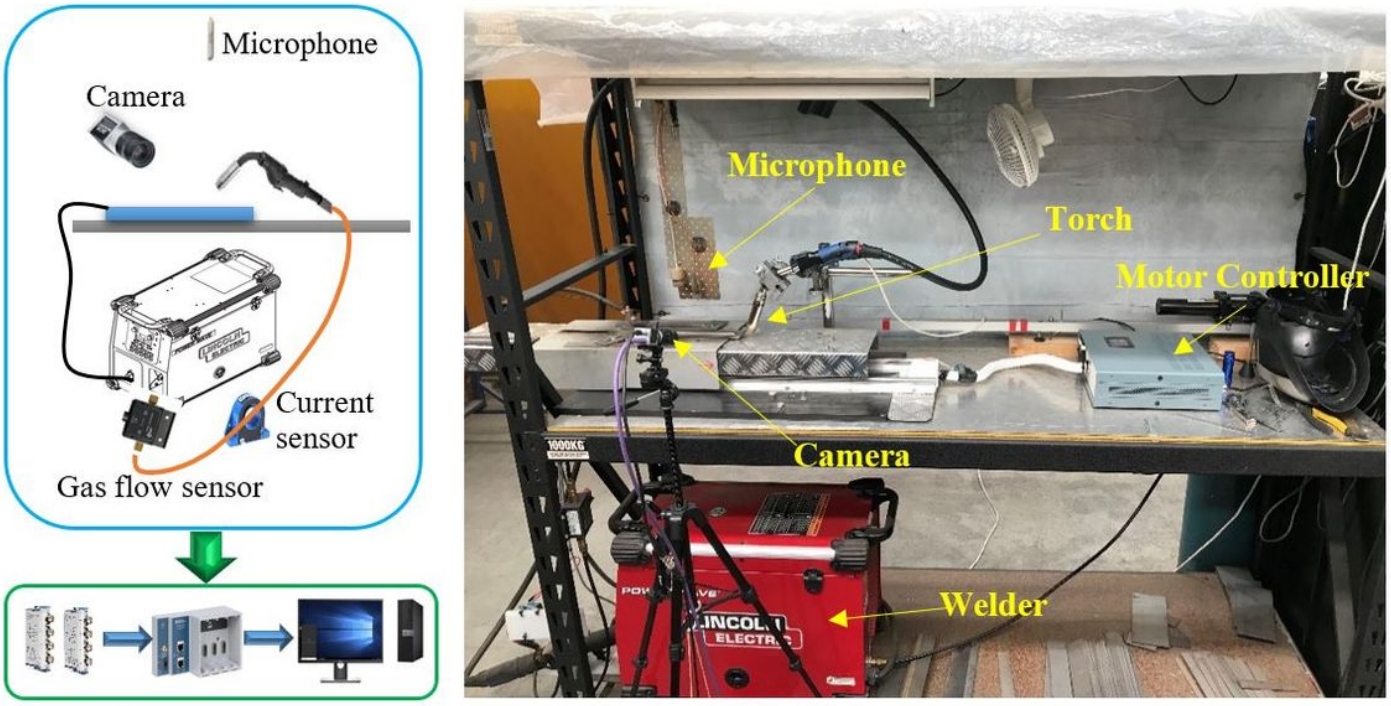

Figure 1

(a) Diagram and (b) photo of the experimental setup for the measurement system

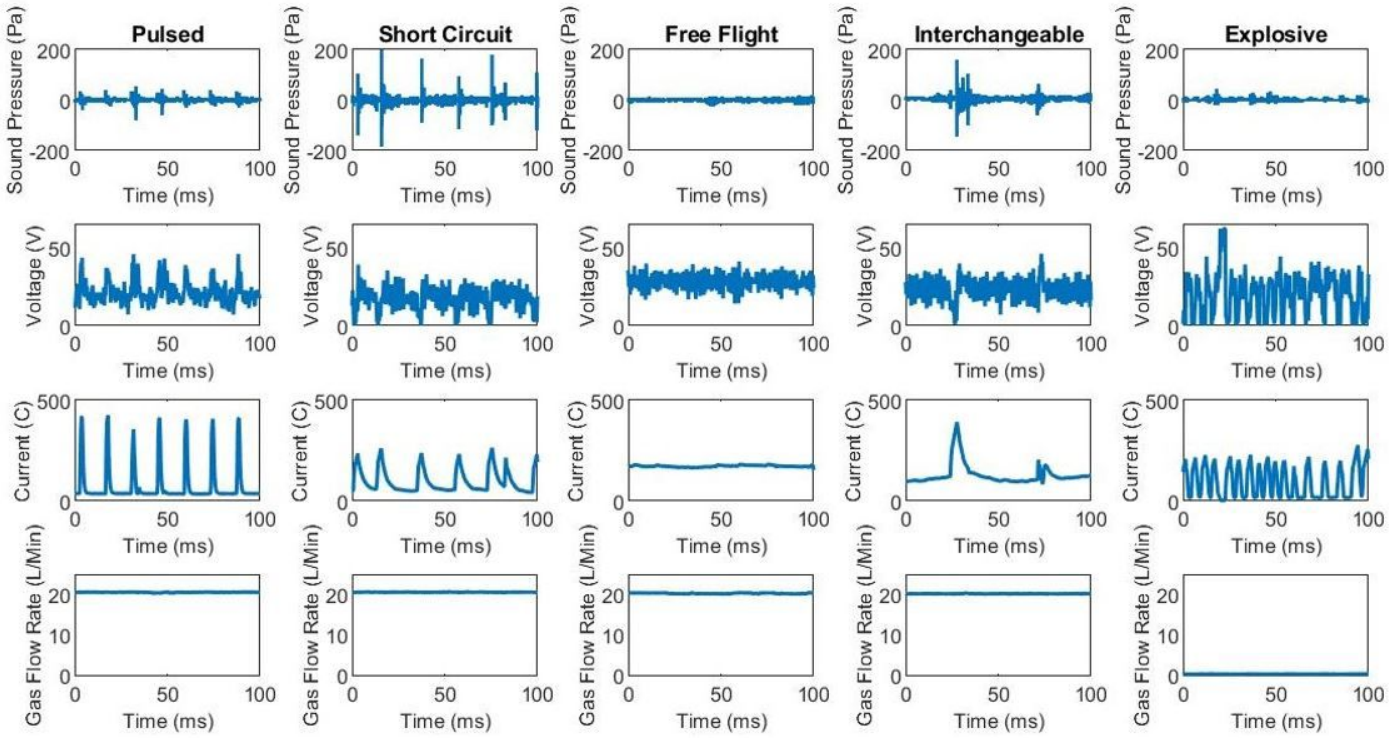

Figure 2

Comparison of the Sound, Voltage, Current and Gas Flow Rate signals for the 5 GMAW Transfer Mode Classifications

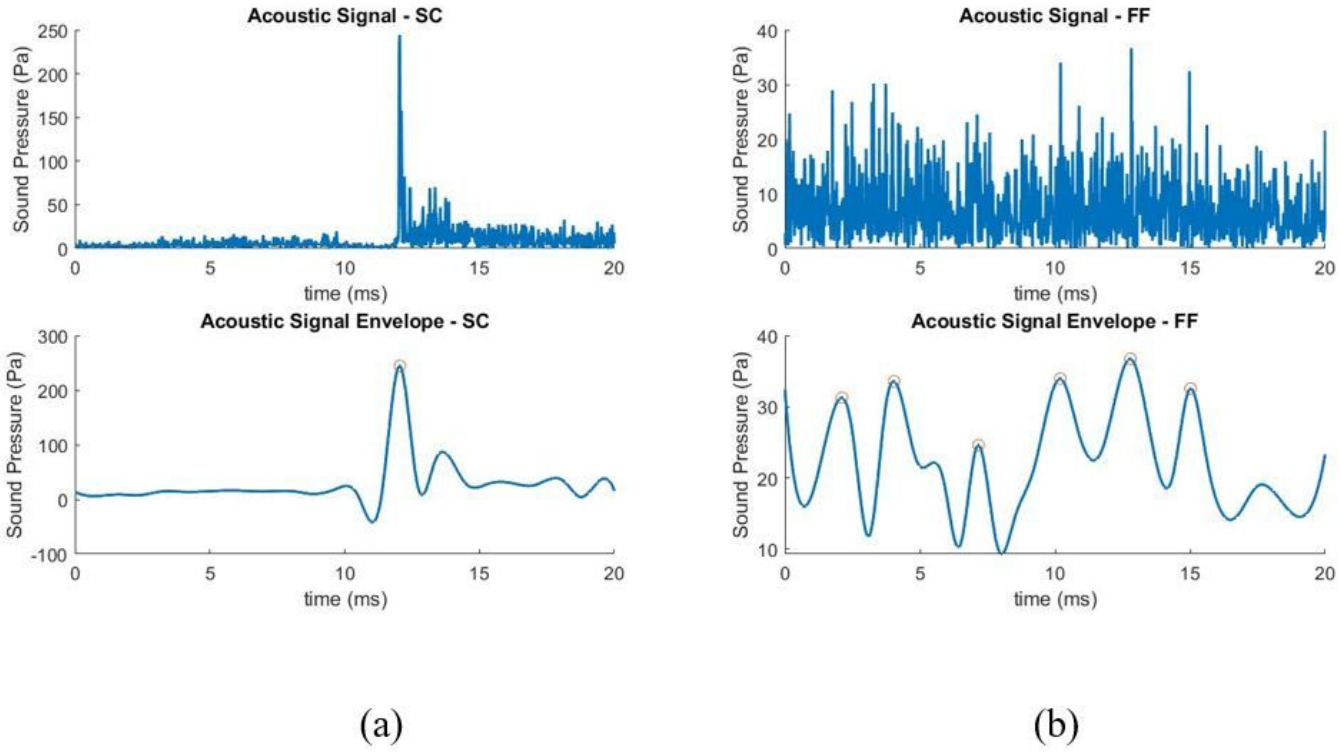

Figure 3

Peak Detection of (a) Short Circuit and (b) Free Flight Transfer

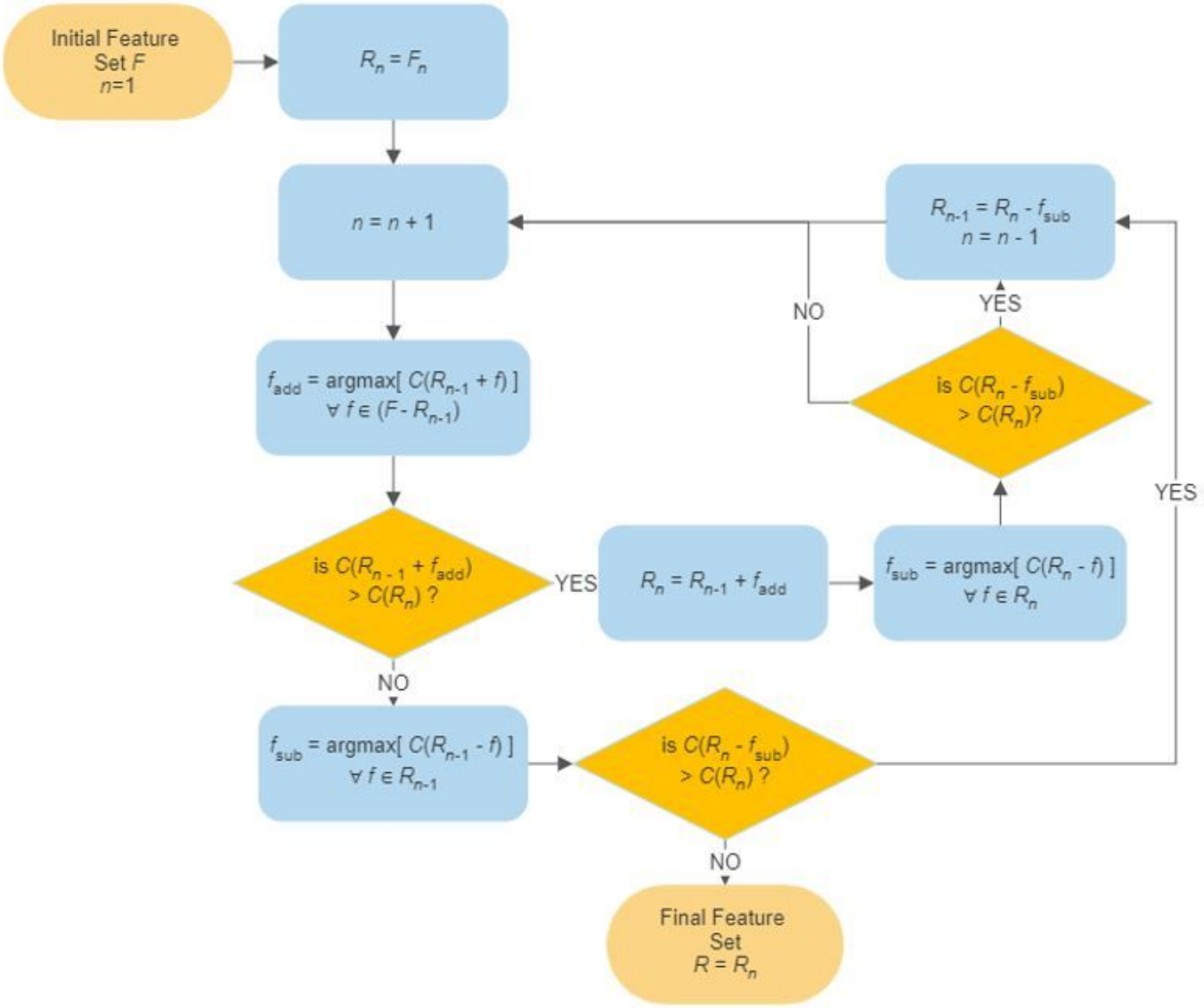

Figure 4

Diagram of the Feature Selection Algorithm

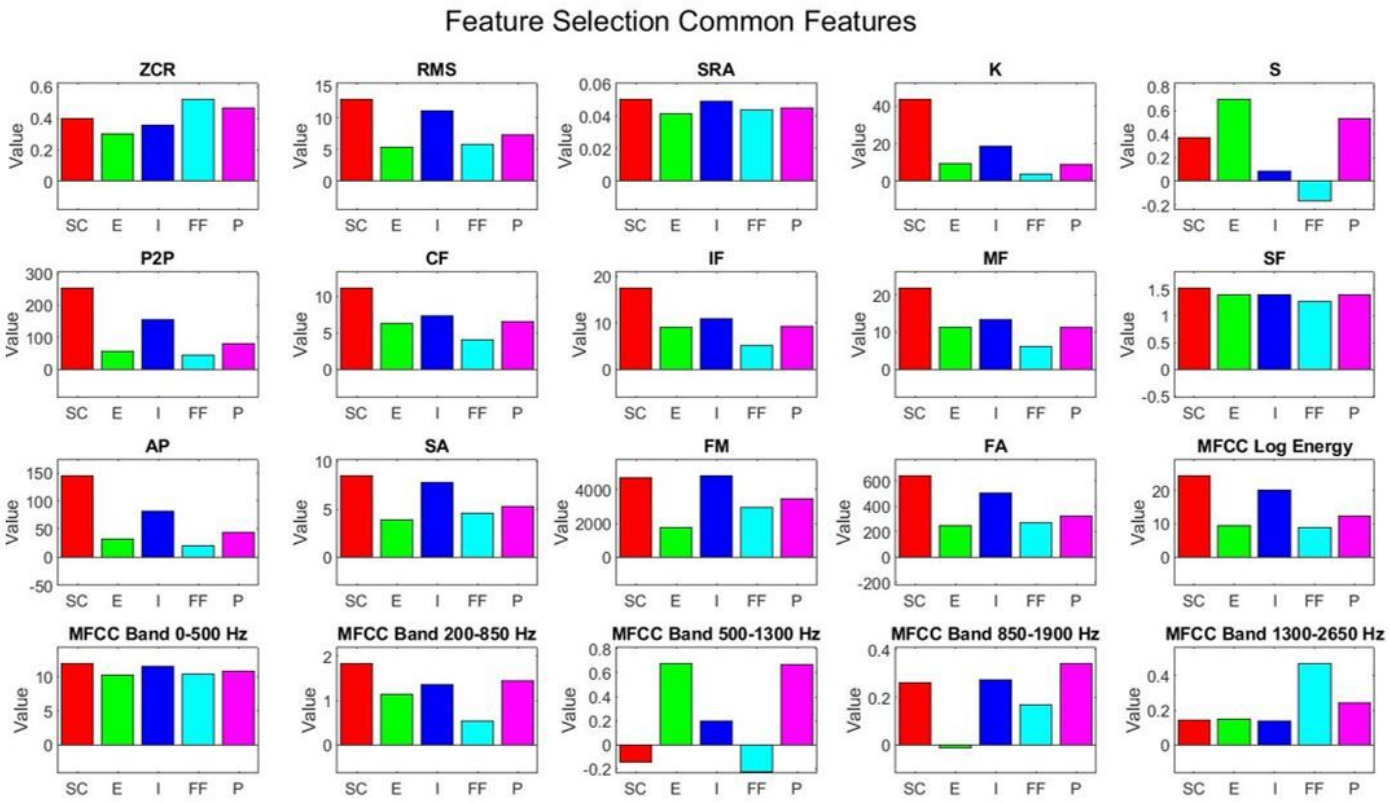

Figure 5

Mean values of Acoustic Features selected by the feature selection algorithm for 20 ms segments.

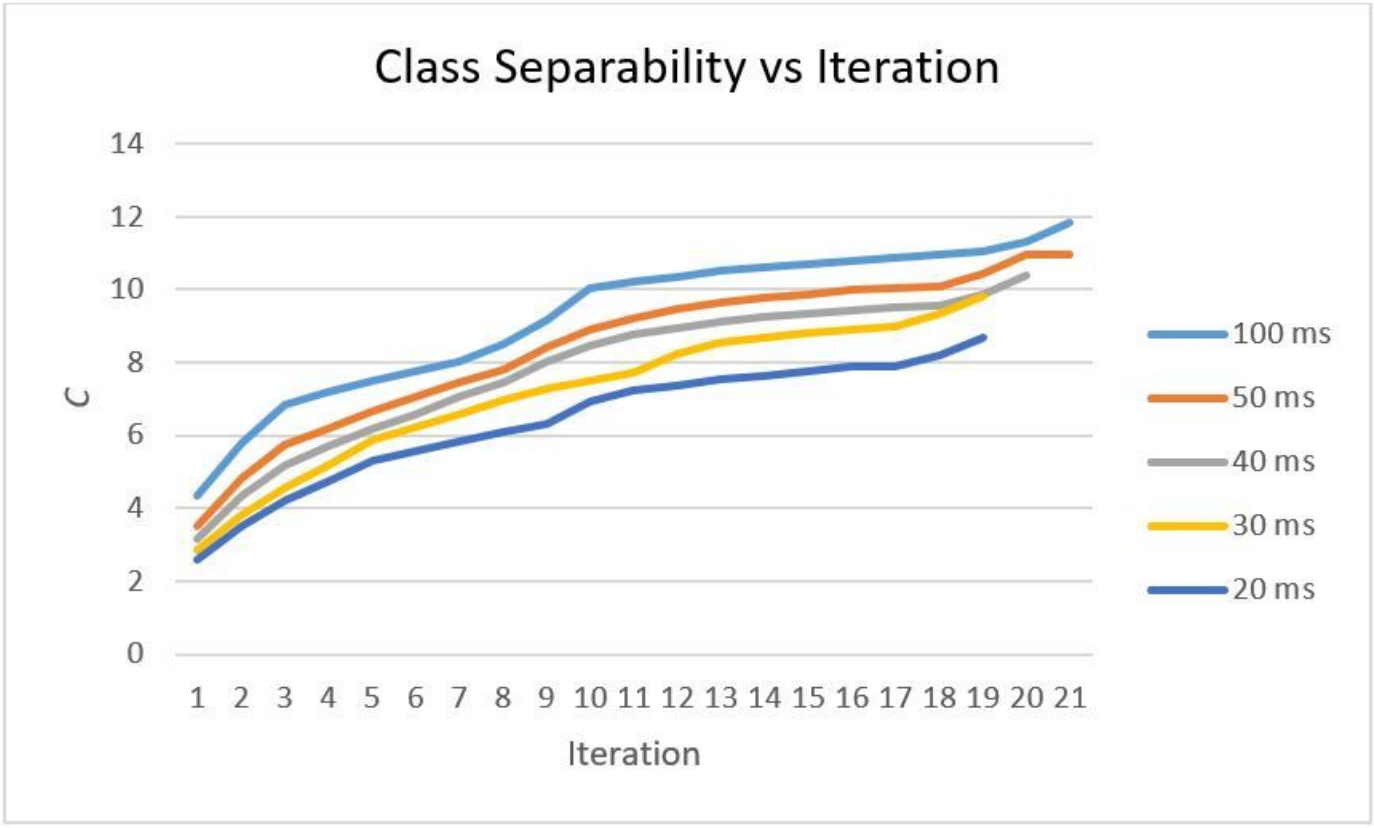

Figure 6

Class separability value C at each iteration of the feature selection algorithm for the acoustic only method

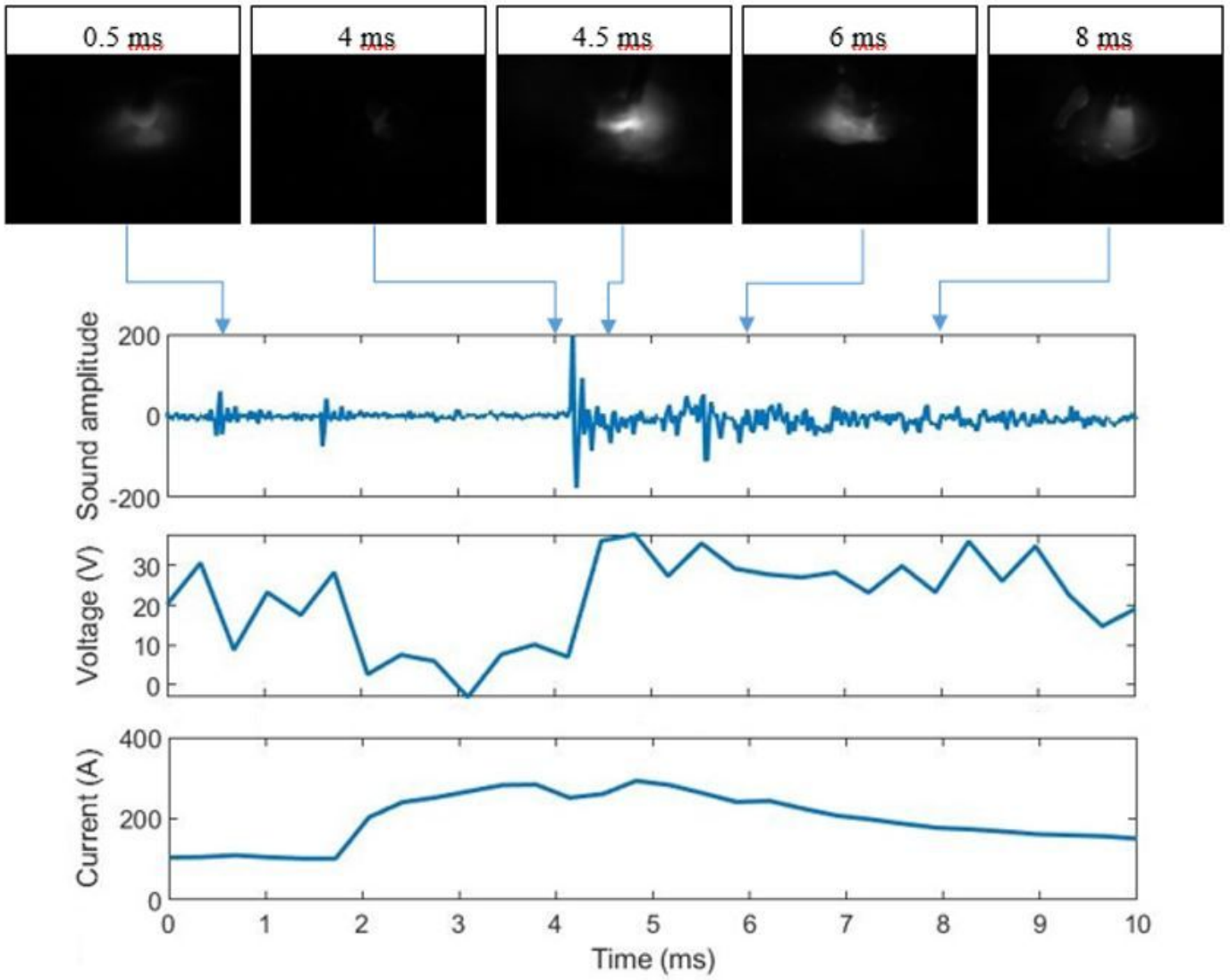

Figure 7

Interchangeable Transfer Mode Signal

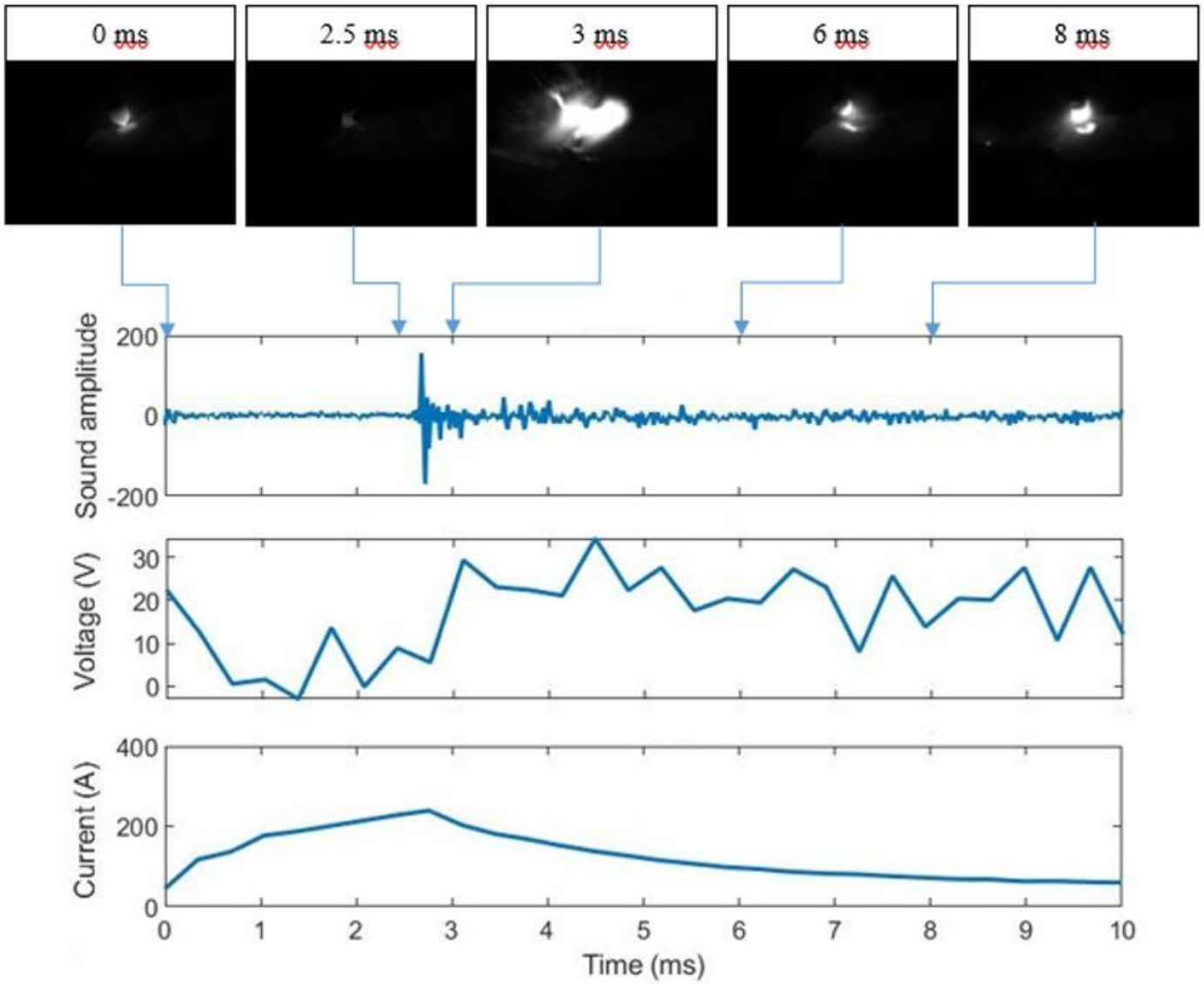

Figure 8

Interchangeable Transfer Mode Signal